Value of a Hydrogen Bond in Triosephosphate Isomerase Loop Motion†

Rebecca B. Berlow,‡ Tatyana I. Igumenova,§ and J. Patrick Loria*,||

Department of Chemistry, Yale University, 225 Prospect Street, New Haven, Connecticut 06520, Department of Molecular Biophysics and Biochemistry, Yale University, 260 Whitney Avenue, New Haven, Connecticut 06520, and Department of Biochemistry and Molecular Biophysics, Columbia University, 630 West 168th Street, New York, New York 10032

Received February 19, 2007; Revised Manuscript Received March 26, 2007

ABSTRACT: The motion of the active site loop (loop 6) in triosephosphate isomerase is investigated in solution by TROSY NMR spin-relaxation experiments. The data show clear evidence for motion with an exchange rate constant (k_{ex}) of 9000 s^{-1}, consistent with opening and closing of this loop being partially rate-limiting to catalytic throughput. Similar rate constants are observed for residues in both the N- and C-terminal regions of loop 6, suggesting motional coupling of the loop hinges. Mutation of tyrosine 208 to a phenylalanine (Y208F) eliminates a hydrogen bond in the closed loop conformation. NMR experiments with this mutant enzyme indicate an increase in the population of the open conformer and concomitant increase in the opening rate constant and a decrease in the rate of loop closure. The destabilization of the closed conformer by ∼3 kJ/mol is consistent with a similar decrease in affinity of Y208F for ligand. The site-specific nature of these experiments leads to additional insight into loop 6 motion and the role of a conserved residue in modulating this motion.

The reversible isomerization between dihydroxyacetone phosphate (DHAP)[1] and glyceraldehyde 3-phosphate (GAP) catalyzed by triosephosphate isomerase (TIM, EC 5.3.1.1) relies in part on the properties of a flexible active site loop (loop 6). Loop 6 in TIM is comprised of 11 residues (166−176) that are highly conserved across numerous organisms (Figure 1). This loop has been shown by biochemical and biophysical studies to be essential for enzymatic function (*1*−*6*). Loop 6 interconverts between open and closed conformations at or near the rate of catalytic turnover, suggesting that its motion is at least partially rate-limiting to the overall enzymatic reaction in the physiologically important DHAP to GAP direction (*7*−*15*). When loop 6 is in the open conformation, the active site is exposed to solvent, thereby allowing substrate to bind or product to be released (*16*). In the closed conformation, loop 6 sequesters the active site and provides a suitable environment for enzyme catalysis to occur (*17*, *18*). Moreover, closure of loop 6 coincides with optimal alignment of the catalytic base E165 with respect to the substrate (*19*). Structural data describing the open and closed forms of loop 6 suggest that this loop moves as a rigid unit. The only significant changes in backbone dihedral angles for the open and closed forms of loop 6 occur in the N- and C-terminal hinges of this loop.

With the exception of a hydrogen bond between the amide NH group of G171 in the center of loop 6 and the phosphate oxygen of substrate, this loop does not interact with the bound ligand (*17*). However, stabilization of the closed form of the loop likely requires several hydrogen bonding interactions between loop 6 and loop 7 (Figure 1). These interactions include H-bonds between A169 O and S211 O^{γ}, G173 N^{H} and S211 O^{γ}, and the N^{H} atom of A176 and the O^{η} atom of Y208. Thus, the energetics that stabilize the closed form of loop 6, in the absence of ligand, result from interactions with loop 7. Biochemical studies of a mutant of TIM (Y208F), in which the hydrogen bond with A176 is absent, confirm the importance of this H-bonding interaction (*2*, *3*). In this mutant, k_{cat} and k_{cat}/K_m are decreased relative to those of WT yeast TIM by 1000- and 2400-fold, respectively. The ability to stabilize the closed form of loop 6 appears to be absolutely essential for optimal catalysis (*3*). However, the role of these residues in loop 6 motion has not been directly investigated.

Solution NMR is uniquely suited to the study of flexible sites in proteins. Motion of a spin-$^1/_2$ nucleus between conformations that have distinct magnetic environments results in a loss of coherent magnetization. This loss manifests as an increase in a measured transverse relaxation rate, R_2, if the time scale of movement is of the appropriate magnitude. Motions in the micro- to millisecond regime will result in decay of spin-locked magnetization and consequently increase the measured R_2 relaxation rate, allowing characterization of the physical parameters that define the motion. A crucial aspect for studies of this kind is the requirement of a difference in the magnetic environment for the NMR nuclei in the two assumed equilibrium conformations. Distinct magnetic environments result in the motionally

† J.P.L. acknowledges NIH Grant R01-GM070823 and the Alfred P. Sloan Foundation. R.B.B. thanks the NIH for biophysical training grant support (5T32GM008283). T.I.I. acknowledges support from NIH Grant DK07328.

* To whom correspondence should be addressed. Telephone: (203) 436-4847. Fax: (203) 432-6144. E-mail: patrick.loria@yale.edu.

‡ Department of Molecular Biophysics and Biochemistry, Yale University.

§ Columbia University.

|| Department of Chemistry, Yale University.

[1] Abbreviations: BMRB, BioMagResBank; cTIM, chicken triosephosphate isomerase; DHAP, dihydroxyacetone phosphate; GAP, glyceraldehyde 3-phosphate; IPTG, isopropyl thiogalactoside; LB, Luria broth; SDS−PAGE, sodium dodecyl sulfate−polyacrylamide gel electrophoresis; TIM, triosephosphate isomerase; TROSY, transverse relaxation optimized spectroscopy.

10.1021/bi700344v CCC: $37.00 © 2007 American Chemical Society
Published on Web 04/25/2007

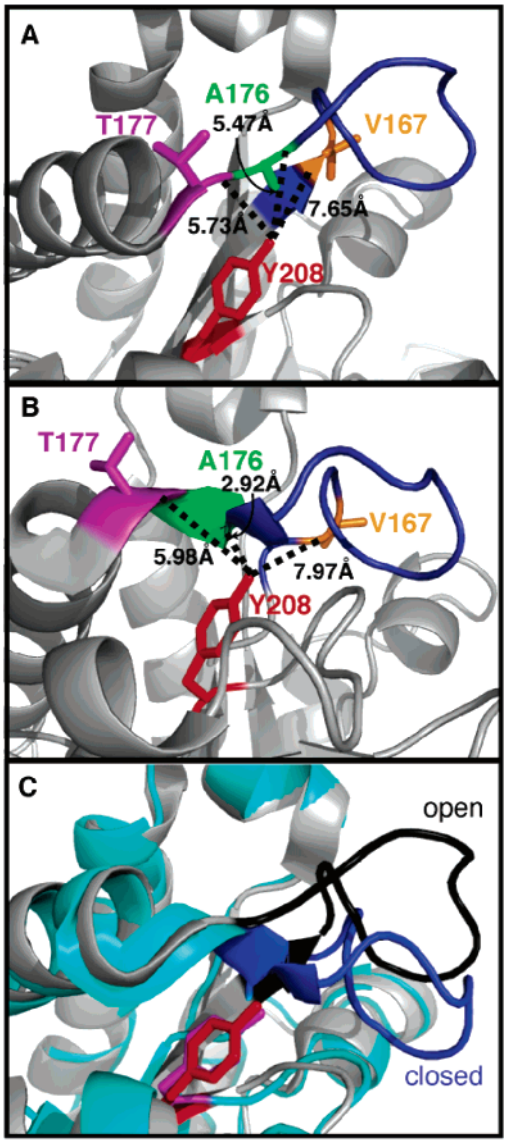

FIGURE 1: Loop 6 in cTIM. Cartoon rendering of the (A) open (*44*) and (B) closed (*45*) conformation of loop 6. The center of loop 6 is colored blue, T177 magenta, A176 green, V167 orange, and Y208 red. Distances between the O^{η} atom of Y208 and the N^{H} atoms of T177, A176, and V167 are indicated by black dashed lines. (C) Overlay of the open and closed conformations of loop 6. Panels A−C were prepared using MacPyMOL (*47*). (D) Primary structure sequence alignment for loop 6 and loop 7 for representative eukaryotic organisms. The N- and C-terminal portions of loop 6 are highlighted in blue and green, respectively. The alignment was prepared using ClustalW (*48*).

averaged atoms experiencing different chemical shifts while they occupy the individual conformations. If there is no chemical shift difference, then motion does not contribute to the measured relaxation rate. Loop 6 motion in chicken TIM (cTIM) is ideally suited for study by this method. As this loop moves between open and closed conformations, significant changes in dihedral angles for residues located in the hinges of loop 6 occur and will therefore result in changes in the local magnetic field sensed by these nuclei. Even though the actual distance traveled by the hinge residues is short (~0.2 Å), the chemical shift changes should be of sufficient magnitude to contribute to the measured relaxation rates (Figure 1A,B). In contrast, the tip of loop 6, which travels approximately 7 Å, is primarily solvent exposed in the open and closed forms. From a solution NMR perspective, residues in the tip of loop 6 may therefore be insensitive to the motion (*20*). In the studies described here, we measure and compare the opening−closing conformational exchange process of loop 6 in wild-type chicken TIM (cTIM) and in the Y208F mutant by solution state NMR relaxation dispersion experiments of the backbone amide positions. These studies identify altered loop 6 motions and suggest a mechanism by which this motion occurs.

MATERIALS AND METHODS

Materials. All reagents were purchased from Sigma (St. Louis, MO) and used in their commercially available forms unless otherwise noted. Stable isotopes for protein expression and labeling were purchased from Isotec/Sigma Aldrich, and D_2O was purchased from Cambridge Isotope Laboratories (Andover, MA).

Plasmids. The plasmid containing the sequence of wild-type chicken TIM cloned into the pET15b bacterial expression vector was a generous gift from N. Sampson (State University of New York, Stony Brook, NY). The Y208F mutant cTIM was prepared by standard PCR-based mutagenesis methods, using the following primers: 5′-GTC-AACTAGGATCATCTTTGGAGGTTCAGTCACTGG-3′ (forward) and 5′-CCAGTGACTGAACCTCCAAAGATG-ATCCTAGTTGAC-3′ (reverse). The correct DNA sequence was confirmed by DNA sequencing (W. M. Keck Facility, Yale University).

Protein Expression and Purification. For the NMR samples (99% ^{2}H, ^{15}N), cultures were grown initially in rich medium (LB) and then successively transferred to M9 minimal medium [0.4% (w/v) glucose] ranging from 50 to 99% D_2O. Uniform ^{15}N labeling was achieved using [^{15}N]ammonium chloride. All cultures were prepared with initial carbenicillin concentrations of 100 μg/mL under standard growth conditions (37 °C and 225 rpm). A single colony was used to inoculate an overnight culture in LB; 1 mL of this culture was added to a small culture of M9 and 50% D_2O and grown to mid-log phase. An aliquot of the M9/50% D_2O culture was then added to a small M9/99% D_2O culture, grown to mid-log phase, and then brought up to the final growth volume in M9 and 99% D_2O. The cultures were grown under standard conditions to an OD_{600} of ~0.6, at which point 800 μM IPTG was added to induce protein expression at 30 °C. Cells were grown for 16−18 h after induction and then harvested by centrifugation.

Escherichia coli cell paste (~2 g per liter of M9/99% D_2O medium) was resuspended in 10 mM Tris-HCl (pH 7.5), and 1 mM PMSF was added as a protease inhibitor. Cells were

lysed by two cycles of sonication. Cell debris was removed by centrifugation. The supernatant was filtered and loaded directly onto a 20 mL FPLC column of DEAE-FF weak anion-exchange resin (Amersham Biosciences/GE Healthcare, Piscataway, NJ) that was pre-equilibrated with 10 mM Tris-HCl (pH 7.5). TIM was eluted with this same buffer and a linear concentration gradient of KCl (from 0 to 150 mM with a total volume of 400 mL) at a flow rate of 2 mL/min. Fractions collected from the FPLC system were analyzed by SDS−PAGE, and cTIM-containing fractions were pooled and desalted using an Amicon concentrator (10 000 MWCO, Amicon, Danvers, MA). Further purification involved an additional pass over the DEAE-FF column. Fractions containing cTIM that were determined to be greater than 95% pure by SDS−PAGE were pooled and concentrated using centrifugal filter devices (Millipore, Billerica, MA). Final protein concentrations were determined using the 280 nm extinction coefficient for cTIM dimer [ϵ_{280} = 44 400 M^{-1} cm^{-1} (*21*)]. Enzymatic activity assays for WT and Y208F cTIM were carried out following the procedure described by Sun and Sampson (*22*), using GAP as a substrate.

Theory. For large proteins, solution NMR measurement of microsecond and millisecond backbone amide motions is aided by the ability to selectively observe transverse relaxation of the slowly relaxing (narrow) component of the NH doublet (R_2^β) (*20*, *23*, *24*). In the rotating frame, relaxation of the amide nitrogen (^{15}N) in the presence of RF irradiation is given by (*24*)

$$R_{1\rho}^\beta = R_1^\beta \cos^2\theta^\beta + R_2^\beta \sin^2\theta^\beta \quad (1)$$

The longitudinal and transverse relaxation rates for the β component of the ^{15}N doublet are

$$R_1^\beta = R_1 - \eta_z + \mu_{^1H} \quad (2)$$

and

$$R_2^\beta = R_2^0 - \eta_{xy} + \mu_{^1H} + R_{ex} \quad (3)$$

in which η_z and η_{xy} are the relaxation interference rate constants for the longitudinal and transverse ^{15}N chemical shielding anisotropy (CSA) and $^{15}N-^1H$ dipole−dipole interactions, respectively, R_2^0 is the exchange-free transverse relaxation rate, and $\mu_{^1H}$ is the cross-relaxation rate constant due to dipolar interactions between $^1H^N$ and remote proton spins, which is minimized by protein deuteration. For perdeuterated macromolecules the size of cTIM, R_2^0 and η_{xy} are approximately equal and $\mu_{^1H}$ is approximately 4 s^{-1}. The conformational exchange contribution (R_{ex}) to the $R_{1\rho}$ relaxation rate constant describes the physical properties of the microscopic motion that give rise to elevated relaxation rates.

$$R_{ex} = \frac{p_A p_B \Delta\omega^2 k_{ex}}{k_{ex}^2 + \omega_e^2} \sin^2\theta^\beta \quad (4)$$

For a two-site conformational exchange model (A ↔ B, k_{close} for the forward direction and k_{open} for backward), p_A and p_B are the equilibrium site populations ($p_A + p_B = 1$) for each conformer, $\Delta\omega$ is the chemical shift difference between the two sites, k_{ex} is the exchange rate constant ($k_{close} + k_{open}$), ω_e is the strength of the effective spin-lock field [$\omega_e = \sqrt{\omega_1^2 + (\Omega^\beta)^2}$], ω_1 is the amplitude of the spin-locking field, Ω^β is the resonance offset of the β component of the NH doublet ($\Omega^\beta = \Omega + \pi J$), and $\theta^\beta = \arctan(\omega_1/\Omega^\beta)$ is the tilt angle of the effective spin-locking field. Measurement of R_2^β as a function of ω_e (known as dispersion analysis) affords characterization of the microscopic exchange parameters for micro- to millisecond motions. For dispersion fitting, R_1^β was measured using the method of Igumenova and Palmer (*24*) and constrained to values bounded by its uncertainty. Using this value, conformational exchange parameters were determined by measuring $R_{1\rho}^\beta$ at several ω_e values, allowing determination of R_2^β at each effective field. In the limit of fast exchange ($k_{ex} > \Delta\omega$), fitting of eq 5 to the relaxation data then yields k_{ex}, ϕ_{ex} (=$p_A p_B \Delta\omega^2$), and $R_2^{0,\beta}$ (*25*).

$$R_2^\beta = \frac{\phi_{ex} k_{ex}}{k_{ex}^2 + \omega_e^2} + R_2^{0,\beta} \quad (5)$$

Alternatively, fitting can be performed with one fewer adjustable parameter by independent measure of R_{ex}^{HE} from a TROSY Hahn echo experiment (*20*) in which

$$R_{ex}^{HE} = p_A p_B \Delta\omega^2 / k_{ex} \quad (6)$$

This value is appropriately substituted into eq 5, and subsequent fitting yields k_{ex} and $R_2^{0,\beta}$.

NMR Studies. All NMR samples were prepared in buffer containing 10 mM MES (pH 6.5), 10 mM NaCl, 7.5% D_2O, and 0.02% (w/v) NaN_3. Sample concentrations were kept below 0.95 mM cTIM dimer to avoid aggregation. Samples for spin-relaxation experiments were uniformly (^2H and ^{15}N) labeled with ~99% isotope incorporation levels as determined by mass spectrometry. NMR experiments were performed at a field strength of 14.1 T on either a Varian Inova 600 MHz spectrometer located at Yale University or a Bruker DRX-600 MHz instrument at Columbia University. Both instruments were equipped with conventional triple-resonance probes. All NMR experiments were conducted at 298 K, which was calibrated using 100% methanol as a standard. All NMR data were processed using NMRPipe (*26*) and analyzed using Sparky (*27*) in conjunction with in-house written programs for dispersion fitting. Backbone resonance assignments from WT cTIM were from BMRB entry 15064 (*4*). For Y208F, the assigned resonances shift by an insignificant amount and were assigned by comparison to the wild-type enzyme. NMR experiments were collected with spectral widths of 2400 × 8000 Hz and 256 × 2048 points in the t_1 and t_2 dimensions for WT and 2500 × 12 000 Hz and 256 × 1024 points in the t_1 and t_2 dimensions for Y208F. Peak heights were quantitated in Sparky using the average of nine points from a 3 × 3 grid centered on the peak maximum (*28*). Relaxation rates were determined from peak intensities and in-house written programs. Uncertainties in rates were determined from duplicate measurements and the Jackknife procedure (*29*). More than 90% of the amide sites in cTIM have been assigned; results reported here are based only on amino acid residues that are not overlapped in the

two-dimensional spectra and that have sufficient signal to noise such that reliable quantitation of peak intensities is possible.

NMR Relaxation Experiments. Off-resonance TROSY-selected $R_{1\rho}$ experiments were performed using the pulse sequence developed by Palmer and co-workers (*24*). The field strength of the spin-locking radio frequency pulse was calibrated prior to each experiment by using off-resonance continuous wave decoupling as previously described (*30*, *31*). The relaxation delays for measuring $R_{1\rho}^{\beta}$ were 2 (×2), 10, 22 (×2), 38, 54, and 80 (×2) ms at each of nine effective field strengths, ω_e for WT and 11 ω_e values for Y208F. The relaxation delay series were conducted with the spin-lock pulse between 5 and 50 ppm upfield of the ^{15}N carrier, utilizing tilt angles ranging from 30° to 65°. The spin-locking relaxation period was surrounded by tan/tanh adiabatic pulses (*32*, *33*) that were used to align magnetization along the respective fields (*34*) and return it to the *z*-axis after the relaxation delay. These adiabatic pulses had a duration of 6 ms and were initiated 15 kHz from the spin-lock carrier frequency. TROSY-detected (in-phase) $R_{1\rho}$ experiments were performed as described previously (*35*). To estimate the exchange contribution to the line width of the ^{15}N β resonance, the TROSY (*36*)-based Hahn-echo experiment was performed as described previously (*20*) using a total relaxation delay of 21.6 ms ($2/J_{NH}$).

Data Analysis. Several fitting methods were used to obtain conformational exchange parameters from the $R_{1\rho}$ relaxation data, and these are described below. First, the conformational exchange process of the N-terminal hinge was assumed to be uncoupled from C-terminal hinge motion. The dispersion data for each hinge were treated separately using two methods. Method 1 involved fitting eq 1 to the $R_{1\rho}$ dispersion data to determine the exchange parameters k_{ex}, ϕ_{ex}, and $R_2^{0,\beta}$. Method 2 utilized the independent measurement of R_{ex}^{HE} as a constant in dispersion fitting by appropriate substitution for ϕ_{ex}. In method 2, there is one less fit parameter as only k_{ex} and $R_2^{0,\beta}$ are determined. These first two methods can yield two distinct k_{ex} values, one for the N-terminal hinge and one for the C-terminal hinge. Second, since much biochemical data suggest that loop 6 moves as a single unit, global fitting of all exchanging residues in loop 6 was performed. In the global model, all residues are restricted to share the same exchange rate constant. In the global dispersion analysis, methods 1 and 2 are identical as described above. Statistical testing was used to make a decision about the more appropriate motional model. This model comparison includes assessing Akaike Information Criteria (AIC) values and *F*-test comparisons, both of which account for the different degrees of freedom in fitting different models to the experimental data. Additional analysis was performed using the results of dispersion fitting combined with estimates of $\Delta\omega^2$ to determine the populations of the exchanging conformations using either the relationship $\phi_{ex} = p_A p_B \Delta\omega^2$ or eq 6 and the independently measured R_{ex}^{HE}. This analysis assumes that the relationship $\Delta\delta^2 = (\delta_{open}^{15N} - \delta_{closed}^{15N})^2$ accurately reflects $\Delta\omega^2$, in which $\Delta\delta$ is the difference in ^{15}N chemical shifts obtained from TROSY spectra of the apo (open, BMRB entry 15064) and bound (closed, BMRB entry 15065) forms of TIM.

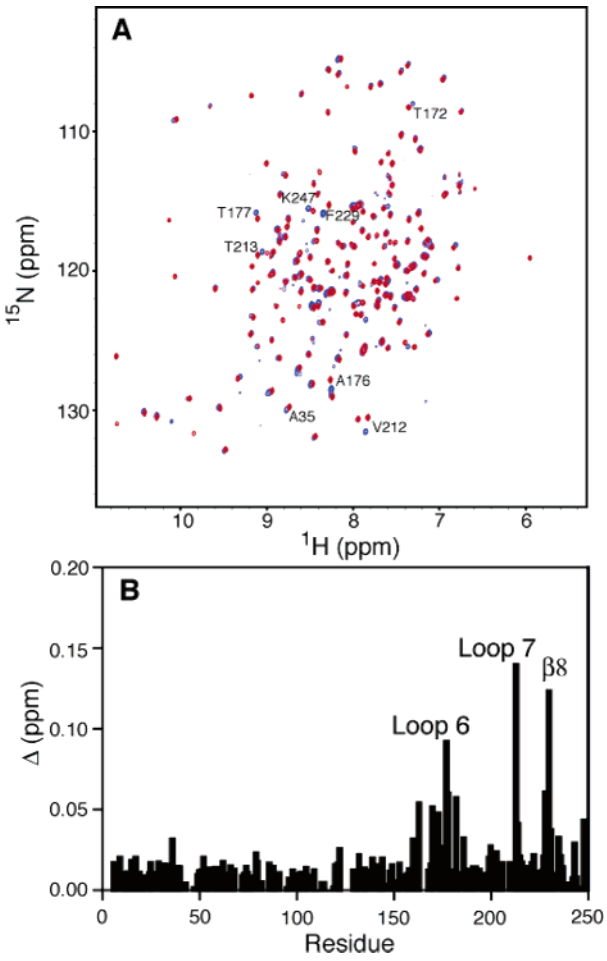

FIGURE 2: Chemical shift changes in cTIM. (A) ^{1}H−^{15}N TROSY (*36*, *49*) spectra of perdeuterated WT (blue) and Y208F (red) cTIM at 298 K and 14.1 T. Selected residues are identified by the single-letter amino acid code. (B) Chemical shift changes [$\Delta = \sqrt{(\Delta\delta_{HN}^2 + \Delta\delta_N^2/25)/2}$] as a function of amino acid sequence, in which $\Delta\delta$ values are the differences in parts per million between WT and Y208F enzymes (*50*). Secondary structure identifiers indicate regions of largest differences.

RESULTS AND DISCUSSION

Enzyme Characterization. Wild-type and Y208F enzymes were expressed and purified to homogeneity as described in Materials and Methods. Enzyme activity assays indicate the expected loss of catalytic activity for the Y208F enzyme (not shown). A comparison of the TROSY ^{1}H−^{15}N correlation spectra (*36*) indicates a high degree of similarity in the overall structures of WT and Y208F enzymes (Figure 2A). Figure 2B highlights the small differences in ^{1}H and ^{15}N chemical shifts (Δ) upon mutation of Y208. These differences are confined to a small number of residues near the site of mutation. When the reaction-intermediate analogue 2-phosphoglycerate binds to WT cTIM, the chemical shifts of loop 6 residues shift (*4*). In the ^{15}N dimension, which is relevant for the discussion given below, the chemical shift change ($\Delta\delta$) is 1460 s^{-1} (3.8 ppm) and 1088 s^{-1} (2.8 ppm) for V167 and T177 in WT and 1444 s^{-1} (3.8 ppm) and 1252 s^{-1} (3.3 ppm) in Y208F, respectively. For K174, the ^{15}N chemical shift changes little upon PGA binding with a $\Delta\delta$ of 76 s^{-1} (0.2 ppm). For Y208F, binding of PGA results in broadening of loop 6 resonances beyond NMR detection, indicating a different kinetic response of loop 6 compared to that of WT.

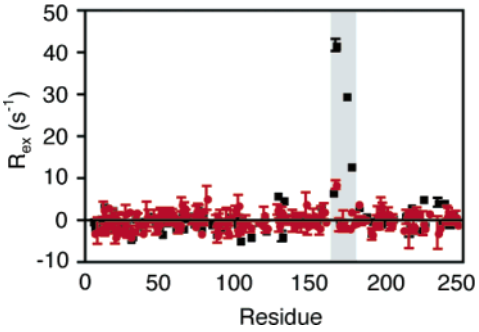

FIGURE 3: Residue-specific chemical exchange contributions to R_2^β. R_{ex}^{HE} was measured for WT (black) and Y208F (red) at 298 K and 14.1 T. A solid black horizontal line is drawn at $R_{ex} = 0$. The shaded gray bar denotes the boundaries of loop 6.

Table 1: Summary of Individual Fits of the NMR Relaxation Experiments[a]

	k_{ex} (s^{-1})	ϕ_{ex} ($\times 10^5$ s^{-2})	p_A	R_{ex} (s^{-1})[g]
WT				
V167[b]	9200 ± 2800	4.14 ± 1.09	0.74 ± 0.19[e]	41.8 ± 1.5
V167[c]	10100 ± 3200	4.22 ± 1.09[d]	0.73 ± 0.23[f]	
K174[b]	4900 ± 1000	1.64 ± 1.05	–	29.6 ± 0.4
K174[c]	4400 ± 200	1.29 ± 0.10[d]	–	
T177[b]	4900 ± 1000	0.56 ± 0.08	0.95 ± 0.14[e]	13.0 ± 0.3
T177[c]	4400 ± 200	0.58 ± 0.10[d]	0.95 ± 0.16[f]	
Y208F				
V167[b]	9800 ± 2300	1.76 ± 0.32	0.91 ± 0.16	8.5 ± 1.0
V167[c]	11500 ± 3500	0.98 ± 0.32[d]	0.95 ± 0.32[f]	
K174	ND[h]	ND[h]	ND[h]	ND[h]
T177	ND[h]	ND[h]	0.99	2.1 ± 0.5

[a] Experimental results from NMR relaxation experiments on the wild-type and Y208F cTIM enzyme. [b] Values determined using method 1 as described in Materials and Methods. [c] Values determined using method 2. [d] Here ϕ_{ex} is given as the product of the independently measured R_{ex}^{HE} with the k_{ex} values in column 2. [e] The fractional population for the major conformer (p_A) was determined using ϕ_{ex} and the assumption that $\Delta\omega^2 = \Delta\delta^2$. [f] The fractional populations were determined using $(R_{ex}^{HE} k_{ex})/\Delta\delta^2$. [g] The exchange contribution to R_2^β was determined as described by Palmer and co-workers (*20*). [h] No dispersion detected. Populations determined for K174 using its $\Delta\delta$ value yield nonphysical results.

Nonetheless, for comparative purposes, we assume, since the open loop chemical shifts for Y208F and WT are nearly identical that the closed form shifts are also likely to be similar.

Conformational Exchange Motions by NMR. To determine the presence of motions at the backbone amide nitrogen sites for the 53 kDa cTIM enzyme, the TROSY Hahn-echo experiment was performed (*20*). In WT and Y208F, the majority of amino acid sites (10% trimmed average, excluding loop 6) show no evidence of exchange broadening: $R_{ex,WT}^{HE} = -0.01 \pm 0.28$ s^{-1} and $R_{ex,Y208F}^{HE} = -0.09 \pm 0.74$ s^{-1} (Figure 3). However, for residues V167 located at the N-terminal hinge of loop 6, K174 in the C-terminal hinge, and T177 positioned just after the C-terminal hinge, R_{ex}^{HE} values are 41.8 ± 1.5, 29.6 ± 0.4, and 13.0 ± 0.3 s^{-1}, respectively, for WT, and in Y208F, these values are 8.5 ± 1.0 and 2.1 ± 0.5 s^{-1} for V167 and T177, respectively (Figure 3 and Table 1). K174 in Y208F is unassigned. This observation of hinge dynamics in WT cTIM is consistent with other studies showing conformational flexibility in loop 6. The absence of exchange contributions to residues in the center of the loop is also consistent with the notion that these "tip" residues behave as a rigid lid; though they are moving, the change in local magnetic environment for these tip residues is minimal such that $\Delta\omega \cong 0$ (*20*). In the apo enzyme, motion between open and closed conformations does not result in substantial changes in ϕ and ψ or hydrogen bonding changes for these tip residues. The same cannot be said for the hinges in which both the backbone dihedral angles change as well as their interactions with other residues. For Y208F, the significant decrease in the measured R_{ex}^{HE} values for V167 and T177 suggests an alteration in the conformational exchange process relative to that of the WT enzyme. Furthermore, the ratio of exchange contributions for each residue ($R_{ex,WT}^{HE}/R_{ex,Y208F}^{HE}$) is very similar, being 5 ± 1 for V167 and 6 ± 1 for T177, indicating that the effects of mutation of Y208 are equally felt by the N- and C-termini of loop 6. Because ^{15}N chemical shifts for Y208F and WT are nearly identical (vide infra), eq 6 predicts that $p_A p_B$ and/or k_{ex} is altered by mutation. These mutation-induced perturbations are examined in more quantitative detail below.

Characterization of loop 6 conformational exchange kinetics was obtained by measurement of $R_{1\rho}$ spin-relaxation rates (*38*) as a function of effective field strength (ω_e), under off-resonance conditions (*39*−*41*). Following eqs 1 and 2, an independent measure of the longitudinal relaxation rate of the narrow doublet component (R_1^β) facilitates the determination of exchange parameters. Thus, R_1^β values were measured using the pulse sequence described by Igumenova and Palmer (*24*). The 10% trimmed average R_1^β values determined for backbone amide sites in WT cTIM and Y208F are 4.3 ± 0.3 and 3.9 ± 0.2 s^{-1}, respectively (Supporting Information). The similarity in these values is consistent with comparable perdeuteration levels between the Y208F and WT enzyme and similar fast time scale dynamics.

The TROSY-selected (TS) off-resonance $R_{1\rho}$ experiment was performed (*24*) for characterization of micro- to millisecond motions in cTIM. The sensitivity improvement and accuracy of this experiment were previously demonstrated for ubiquitin, and calculations showed the expected benefits for higher-molecular weight systems (*24*). In Figure 4, the excellent sensitivity of this experiment on WT cTIM is demonstrated and compared to that of the TROSY-detected (in-phase) $R_{1\rho}$ experiment (*35*). The additional signal to noise of the TS experiment at large tilt angles and longer relaxation times is evident from these data. Representative TS−$R_{1\rho}$ decay curves for selected residues are shown in Figure 5. Multiple decay curves such as those shown in Figure 5 were obtained at varying ω_e values for dispersion analysis.

The dispersion data for residues V167, K174, and T177 in WT cTIM were analyzed using the fitting methods described. Measured rates at all effective field strengths are provided in the Supporting Information. The results for the independent and global fitting protocols are listed in Tables 1 and 2, respectively. When V167 is analyzed separately from K174 and T177, very different k_{ex} values are obtained for the N- and C-termini of loop 6 (Figure 6). V167 has an exchange rate constant of ~10000 s^{-1}, whereas K174 and T177 have a k_{ex} value of ~5000 s^{-1}. It is reassuring that nearly identical results are obtained regardless of whether R_{ex}^{HE} is used as a restraint. This indicates the fitting is robust and the system not underdetermined.

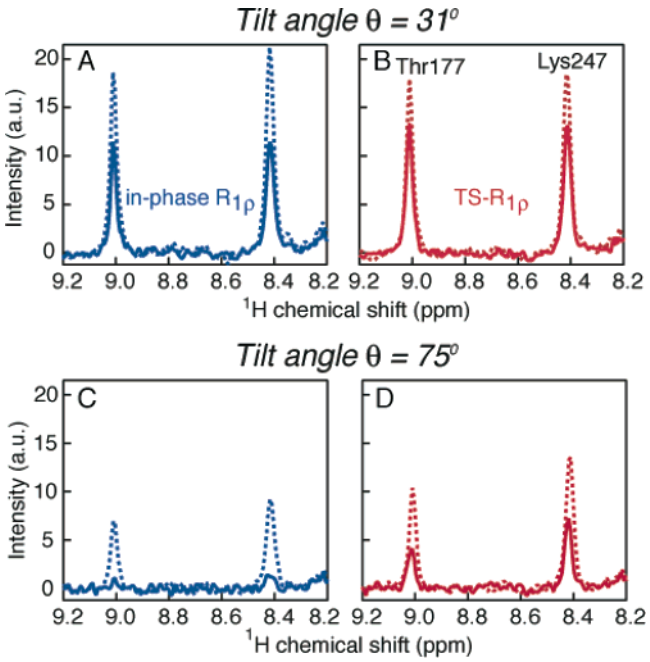

FIGURE 4: Comparison of TS−$R_{1\rho}$ vs TD−$R_{1\rho}$ (in phase). One-dimensional (^{1}H) slices through the peaks for resonances T177 and K247 in WT cTIM for in-phase $R_{1\rho}$ (A and C) (*35*) and the TROSY-selected $R_{1\rho}$ (B and D) (*24*). The dashed lines correspond to relaxation delays of 30 ms, whereas the solid lines represent 80 ms relaxation delays for tilt angles (θ) of 31° (A and B) and 75° (C and D). The data were acquired at 14.1 T and 298 K.

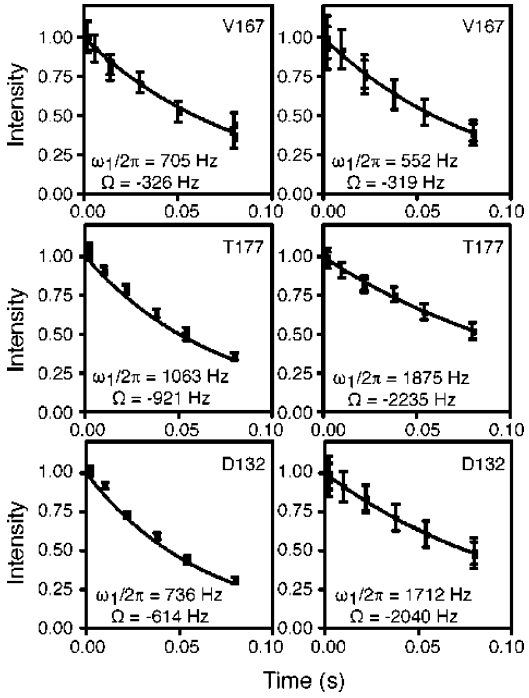

FIGURE 5: Decay of spin-locked magnetization. Representative $R_{1\rho}$ decay curves for WT (left) and Y208F (right) are shown with the solid line indicating the best fit of a single-exponential decay to the data. The bottom left corner of each graph provides the magnitude of the spin-lock field and the frequency offset for each experiment. The identity of the amino acid residue is provided at the top of each graph. For WT residues V167, T177, and D132, $R_{1\rho}$ values are 11.7 ± 1.6, 13.8 ± 0.6, and 15.7 ± 0.5 s^{-1} for tilt angles of 65°, 50°, and 50°, respectively. In Y208F, these values are 11.8 ± 1.8, 8.1 ± 0.9, and 9.1 ± 1.6 s^{-1} at tilt angles of 60°, 40°, and 40°, respectively.

The $R_{1\rho}$ dispersion data were also analyzed using a global model in which all residues possess the same exchange rate constant. Those data are presented in Table 2 and Figure 6. The k_{ex} value for loop 6 motion for the global model is 8900 s^{-1}. By standard AIC (*42*) and *F*-test (*43*) criteria, the global model is better than treating the hinges separately. Comparison of the independent and global models using method 1 protocols gives a ΔAIC of 3 and a *P* of 0.15, indicating that the global model is the most appropriate fitting model. When the comparison is performed between the independent and global fits obtained with method 2, both models appear to describe the data equally well; the global model, being simpler, is the accepted model. Thus, the NMR dispersion data indicate that loop 6 hinges interconvert between the open and closed forms with identical rate constants. These data are consistent with loop 6 hinges moving in a concerted fashion. The exchange rate constant determined here is consistent with measured exchange rates determined from other studies on the highly homologous yTIM (*8*−*10*, *13*, *14*). In addition, this measured exchange rate constant is of the appropriate time scale to contribute to the rate-limiting step in the TIM reaction (*15*). In WT cTIM, two additional residues, G128 and D132, both have an R_{ex}^{HE} of >0 (Figure 3) and also have measurable dispersion curves (not shown), though the exchange parameters are different from those observed for V167 and T177.

Dispersion curves for Y208F are also shown in Figure 6C. Only V167 can be quantitatively analyzed because no dispersion profile is observed for T177 and residue K174 is not assigned in this mutant. Both fitting methods give similar results for V167. A k_{ex} value of approximately 10 000 s^{-1} is obtained and is statistically indistinguishable from the WT k_{ex}. Y208 appears to play an equal role in the opening and closing rate constants of loop 6. The decrease in ϕ_{ex} for Y208F relative to that of the WT enzyme reflects a shift in the conformational equilibrium toward the open form. These data indicate that the loop 6 opening rate increases and the closing rate decreases, thereby maintaining a WT-like k_{ex} value, but increasing the equilibrium amount of open loop 6. In contrast to observations with the WT enzyme, no dispersion of R_2^{β} with ω_e is observed for T177. This is consistent with the decrease in R_{ex}^{HE} (2.1 ± 0.5 s^{-1}) for T177 upon mutation (Figure 3). As a check of the robustness and internal consistency of the dispersion results, ϕ_{ex}/k_{ex} determined from the dispersion analysis gives values very similar to the independently determined R_{ex}^{HE} values for both WT

Table 2: Summary of Global Fits of the NMR Relaxation Experiments for WT cTIM[a]

residue	k_{ex} (s^{-1})	ϕ_{ex} ($\times 10^5$ s^{-2})	p_A
V167[b]	8900 ± 1600	4.12 ± 0.63	0.74 ± 0.17
K174[b]		1.61 ± 0.39	*e*
T177[b]		0.94 ± 0.30	0.91 ± 0.33
V167[c]	8800 ± 1700	3.68 ± 0.71[d]	0.78 ± 0.21[f]
K174[c]		2.61 ± 0.50[d]	*e*
T177[c]		1.14 ± 0.22[d]	0.89 ± 0.24[f]

[a] Experimental results from NMR $R_{1\rho}$ relaxation experiments on wild-type cTIM using a global dispersion model in which k_{ex} is shared by V167, K174, and T177. [b] Relaxation data were analyzed using method 1. [c] Relaxation data were analyzed using method 2. [d] Here ϕ_{ex} is given as the product of the independently measured R_{ex}^{HE} with the k_{ex} values in column 2. [e] No reliable Δδ data are available for this residue. [f] The fractional populations were determined using $(R_{ex}^{HE}k_{ex})/\Delta\delta^2$.

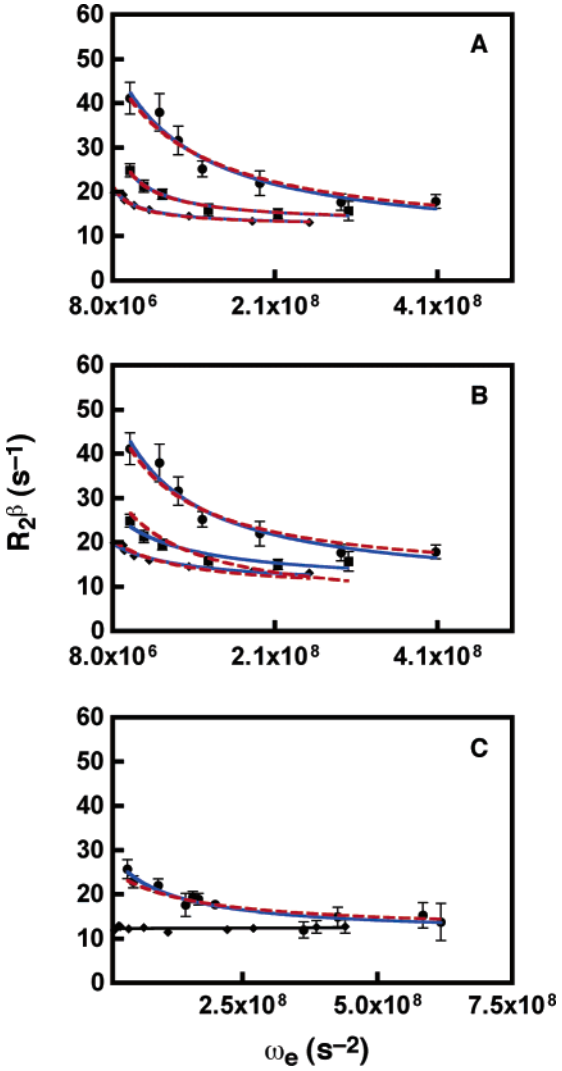

FIGURE 6: Conformational exchange in cTIM. TROSY-selected $R_{1\rho}$ dispersion curves for V167 (●), K174 (■), and T177 (◆) for WT (A and B) and Y208F (C) cTIM. In panel A, the curves represent the best fit to the dispersion data treating the N- and C-terminal portions of the loop 6 hinge separately. The curve for method 1 is shown as a solid blue line and that for method 2 as a dashed red line. In panel B, the curves are those for the global fit of all three residues to a single conformational exchange process with the color scheme identical to that in panel A. In panel C, the same color scheme is used to depict dispersion data for V167 in the Y208F enzyme, with the exception of the data for T177, which were fitted with a linear function with a slope of 0. The fit parameters are provided in Tables 1 and 2.

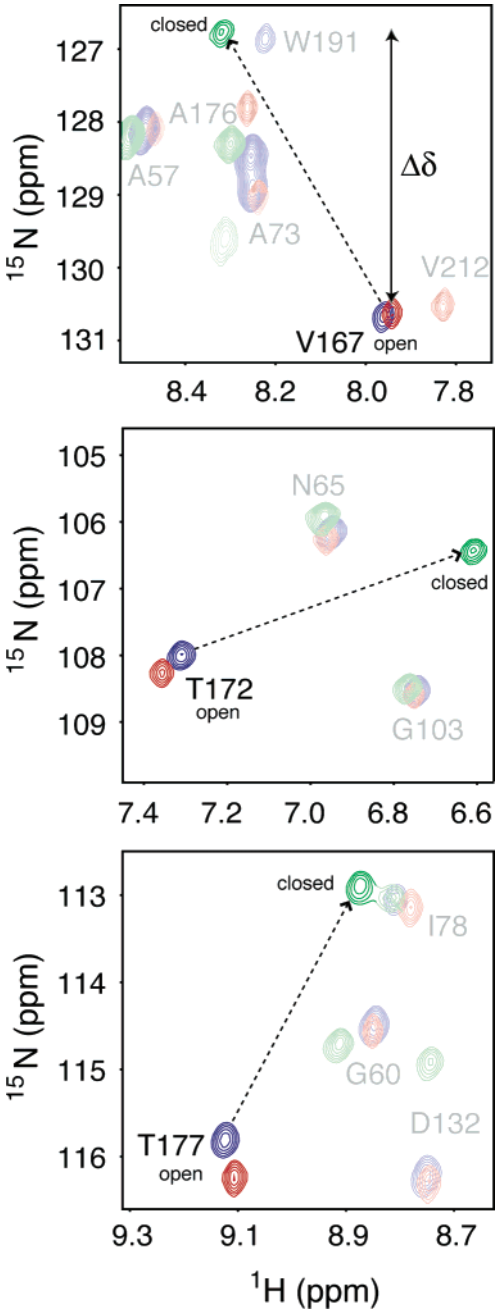

FIGURE 7: Magnitude of conformational exchange. The chemical shift changes for loop 6 residues are shown for V167 (top), T172 (center), and T177 (bottom) for WT in the open (blue) and closed (green) conformations. The open conformation for Y208F is colored red. The value of $\Delta\delta$ as reported in the text is represented by the vertical arrow in the top panel.

and Y208F. Additional analysis of the loop 6 motion can be obtained from ϕ_{ex}, which can lead to estimation of the fractional populations for the major, open and minor, closed conformations from the relationship $p_A - p_A^2 = \phi_{ex}/\Delta\omega^2$.

Wild-Type Chemical Shifts and Populations. The backbone chemical shifts for WT cTIM in the open and closed conformations were determined previously (BMRB entries 15064 and 15065, respectively) (*4*). In the absence of substrate, WT loop 6 exists primarily in the open conformation (*44*, *45*), though solid state (*8*) and solution state NMR (*4*, *9*, *10*, *13*, *20*) indicate that this loop interconverts between open and closed forms. Likewise, in the ligand-bound form, the loop moves between the major, closed conformer and the open state (*9*, *10*, *13*). For a spin-$^1/_2$ nucleus undergoing a two-site conformational exchange process in the fast limit, the observed resonance position, ω_{obs}, is given by the relation $\omega_{obs} = p_A\omega_A + p_B\omega_B$ in which ω_A and ω_B are the chemical shifts for the nuclei in conformations A and B, respectively, and $\Delta\omega = |\omega_A - \omega_B|$. Thus, for WT cTIM, in solution, the chemical shifts for resonances in loop 6 reside at a position determined by the population-weighted average of the open and closed forms. Moreover, comparison of the differences in ^{15}N chemical shifts in the two-dimensional ^{1}H−^{15}N spectra of open and closed forms of cTIM provides $\Delta\delta = |\delta_{open} - \delta_{closed}| \cong \Delta\omega$ (Figure 7). For WT cTIM, the magnitude of ϕ_{ex} and R_{ex}^{HE} correlates well with $\Delta\delta^2$, suggesting that $\Delta\delta$ is a good approximation of $\Delta\omega$. This correlation does not extend to K174. Using this approximation leads to an

estimation of the fractional populations for the WT enzyme: $p_A^{V167} = 0.74-0.78$ and $p_A^{T177} = 0.89-0.91$ (Table 2). This analysis indicates perhaps the N- and C-terminal hinges behave in a somewhat independent fashion. Though the uncertainties are significant, it remains surprising that identical populations are not observed for the N- and C-terminal residues of loop 6. However, given the large uncertainties and the uncertainty in the exact value of $\Delta\omega$, it is at present not clear if these represent real differences in equilibrium populations. The notion of relatively independent loop 6 hinges is somewhat unusual, yet a crystal structure of the homologous *Leishmania mexicana* TIM at 0.82 Å resolution shows significant anisotropy in the C-terminal hinge but not in the N-terminal region (*46*). In addition, computational experiments indicate that the H-bonds that stabilize the N- and C-terminal hinges break at different times (*12*, *13*). Furthermore, Sampson and co-workers, using site-directed mutagenesis of the amino acid residues in the cTIM hinges, addressed sequence requirements for hinge function. Many of the double (N and C) mutants had synergistic decreases in the free energy of activation for catalysis, indicating interdependence of the loop 6 hinges (*6*). However, five of the double mutants that were studied possessed additive losses in activity relative to the individual mutations. This result indicates that at some level the N- and C-terminal hinges operate independently and is consistent with our NMR dynamics results; however, more experiments are necessary to confirm such a novel view of loop 6 motion.

Y208F Chemical Shifts and Populations. The ^{15}N chemical shifts in Y208F change little from the WT values, consistent with the minor structural perturbation expected from a tyrosine to phenylalanine substitution. This similarity further suggests that the WT values for $\Delta\delta \cong \Delta\omega$ are appropriate for the mutant as well. The chemical shifts for loop 6 residues in unliganded Y208F are compared to these WT chemical shift values (Figure 7). As noted above, the similarity of the chemical shifts for Y208F and WT indicates that loop 6 in apo-Y208F, like that in apo-WT, exists predominantly in the open conformation. In apo-Y208F, however, the ^{15}N chemical shifts are slightly farther from the closed conformation chemical shifts than those of apo-WT, suggesting a subtle shift in the equilibrium population distribution toward the open form (Figure 7). The small changes in ^{1}H chemical shifts additionally suggest other minor changes to loop 6; if mutation simply resulted in an increase in the level of the open conformation the Y208F, ω_{obs} should be "in line" with the WT open and closed shifts. Nonetheless, the observation that the magnitudes of ϕ_{ex} and R_{ex}^{HE} decrease upon mutation likely reflects a shift in the population distribution that is skewed toward the open form.

Performing the same analysis for Y208F as WT gives a fractional population for the major conformer of 0.91 ± 0.16 for V167. Because the mutation affects the R_{ex}^{HE} values of V167 and T177 by a factor of 5−6, the fractional population of T177 increases by the same amount and would be 0.99 (Table 1). Thus, the general conclusion is that removal of a hydrogen bond by mutation of Y208 increases the population of the open conformer of loop 6 by a magnitude similar to that of the increase and decrease in k_{open} and k_{closed}, respectively. The observation that removal of a stabilizing interaction at the C-terminus of loop 6's hinge affects the open−closed equilibrium at the N-terminal hinge indicates that these two hinge regions are motionally coupled. The analysis of the WT data and that for Y208F point to unequal population distributions for the N- and C-terminal hinges; however the mutagenesis data indicates some coupling of the N- and C-terminal hinge movement because mutation near the C-terminal side also affects the dynamics at the N-terminal side of the loop.

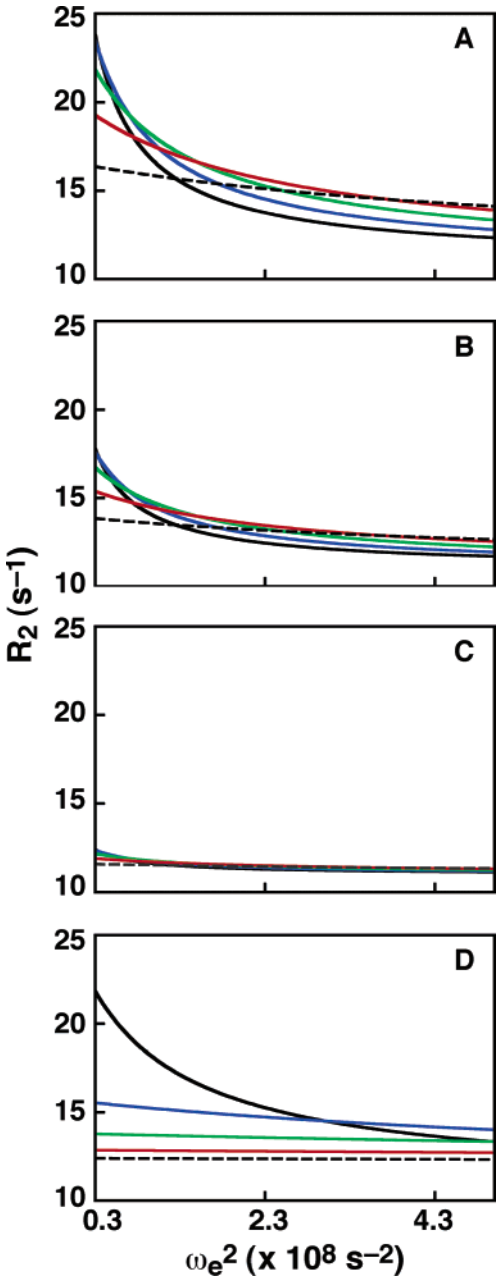

FIGURE 8: Simulated $R_{1\rho}$ dispersion curves for T177 in Y208F. Dispersion curves are shown for a two-site exchange model with population distributions of (A) 90:10, (B) 95:5, (C) 99:1, and (D) 90:10 for a single residue with exchange parameters similar to those expected for T177. In each case, ϕ_{ex} was 1.14×10^5, 7.46×10^4, 1.55×10^4, and 1.14×10^5 s^{-2} for panels A−D, respectively, using a $\Delta\omega$ of 1250 s^{-1}. In panels A−C, curves are obtained using k_{ex} values of 25 000 (black dashed), 15 000 (red), 10 000 (green), 7000 (blue), and 5000 s^{-1} (black solid). For panel D, $k_{ex} = 10\,000$ (black solid), 30 000 (blue), 50 000 (green), 75 000 (red), and 10 000 s^{-1} (black dashed). Simulated data were generated using Prism 4.0 (Graphpad, San Diego, CA).

The measurement in Y208F of an R_{ex}^{HE} of >0 for T177 is evidence for conformational exchange motion, yet no $R_{1\rho}$ dispersion is observed for this residue. This is not due to scatter in the data obfuscating a small magnitude of exchange contributions but rather a highly skewed population ratio as described above and/or, potentially though less likely, a greatly elevated k_{ex}. To address the conditions under which conformational exchange for T177 would be unobservable, a series of simulations were performed (Figure 8). These simulated data indicate that for a major population $p_A = 90\%$, k_{ex} values of up to 30 000 s^{-1} (Figure 8A,D) are readily detected, and when $p_A = 95\%$, a k_{ex} of 25 000 s^{-1} (Figure 8B) should be measurable. However, for more highly skewed populations ($p_A = 99\%$), even a k_{ex} of 5000 s^{-1} (Figure 8C) would be impossible to measure with the effective fields used in this study. These simulations support, as suggested from the NMR experiments, that the C-terminal side of loop 6 in Y208F exists in the open conformation approximately 99% of the time. In addition, even in Y208F, there appear to be unequal fractional populations for the open form of the N- and C-terminal hinges because these simulations indicate that our experiments would have detected dispersion in a 90:10 population distribution with the expected k_{ex} value.

Reconciliation of altered loop motion and altered enzyme function in Y208F requires consideration of loop motion in the overall catalytic scheme. The Michaelis constant for DHAP and the K_i for the substrate-like inhibitor glycerol 3-phosphate are nearly identical, suggesting that substrate K_m is a reasonable thermodynamic constant (*5*, *13*). In addition, a normal deuterium isotope effect for [1(*R*)-^{2}H]-DHAP has been measured, indicating that chemistry is part of the rate-limiting step(s). Because the open form has a lower affinity for the ligand than the closed form (*1*), destabilizing the closed conformation should decrease the affinity of TIM for its ligand. On the basis of these NMR data, removal of the hydrogen bonding interaction between Y208 and A176 destabilizes the closed conformation by approximately 3.5 kJ/mol. It is observed in Y208F that the K_m value for substrate is elevated relative to that of the WT enzyme. The relative loss of affinity of TIM for substrate is 3 kJ/mol (*3*). If these disrupted loop 6 populations persist in the enzyme−ligand complex, they should also be directly responsible for the loss of catalytic activity because catalysis occurs only when loop 6 is closed. Confirmation of this awaits further NMR studies on the ligand-bound Y280F cTIM.

CONCLUSIONS

TROSY-selected off-resonance $R_{1\rho}$ experiments provide sufficient sensitivity for quantitating conformational exchange processes in proteins at least as large as 53 kDa. These experiments were used to characterize active site loop 6 motion in cTIM. Measured exchange rates are consistent with loop 6 motion being partially rate-limiting to the overall enzymatic reaction. Analysis of the mutational effects on loop 6 motion indicates that removing the Y208−A176 H-bond near the C-terminal hinge affects the populations of both hinges to a similar extent, destabilizing the closed conformer by ~3 kJ/mol relative to WT. The similar effects at both hinge positions suggest an interdependence of hinge motion, yet analysis of fractional populations of open and closed loop forms in WT suggests different equilibrium values for the N- and C-terminal hinges, indicating some degree of independence for these two regions. Simulation and experiment indicate that for the C-terminal hinge in Y208F the populations are so highly skewed toward the open conformation that observation by these dispersion experiments is not possible, whereas the equilibrium populations of the open and closed forms for the N-terminal hinge do not preclude their measurement. The role of the substrate or inhibitor in modulating hinge motion should provide additional insight into this process.

ACKNOWLEDGMENT

We thank Professor Arthur G. Palmer (Columbia University) for the use of his Bruker 600 MHz NMR instrument.

SUPPORTING INFORMATION AVAILABLE

Table of residue-specific R_1^β values and $R_{1\rho}^\beta$ values at each offset. This material is available free of charge via the Internet at http://pubs.acs.org.

REFERENCES

1. Pompliano, D. L., Peyman, A., and Knowles, J. R. (1990) Stabilization of a reaction intermediate as a catalytic device: Definition of the functional role of the flexible loop in triosephosphate isomerase, *Biochemistry 29*, 3186−3194.
2. Sampson, N. S., and Knowles, J. R. (1992) Segmental motion in catalysis: Investigation of a hydrogen bond critical for loop closure in the reaction of triosephosphate isomerase, *Biochemistry 31*, 8488−8494.
3. Sampson, N. S., and Knowles, J. R. (1992) Segmental movement: Definition of the structural requirements for loop closure in catalysis by triosephosphate isomerase, *Biochemistry 21*, 8482−8487.
4. Kempf, J. G., Ju-yeon, J., Ragain, C., Sampson, N. S., and Loria, J. P. (2007) Dynamic requirements for a functional protein hinge, *J. Mol. Biol.* (in press).
5. Xiang, J. Y., Jung, J. Y., and Sampson, N. S. (2004) Entropy effects on protein hinges: The reaction catalyzed by triosephosphate isomerase, *Biochemistry 43*, 11436−11445.
6. Xiang, J., Sun, J., and Sampson, N. S. (2001) The importance of hinge sequences for loop function and catalytic activity in the reaction catalyzed by triosephosphate isomerase, *J. Mol. Biol. 307*, 1103−1112.
7. Maister, S. G., Pett, C. P., Albery, W. J., and Knowles, J. R. (1976) Energetics of triosephosphate isomerase: The appearance of solvent tritium in substrate dihydroxyacetone phosphate and in product, *Biochemistry 15*, 5607−5612.
8. Williams, J. C., and McDermott, A. E. (1995) Dynamics of the flexible loop of triosephosphate isomerase: The loop motion is not ligand gated, *Biochemistry 34*, 8309−8319.
9. Rozovsky, S., Jogl, G., Tong, L., and McDermott, A. E. (2001) Solution-state NMR investigations of triosephosphate isomerase active site loop motion: Ligand release in relation to active site loop dynamics, *J. Mol. Biol. 310*, 271−280.
10. Rozovsky, S., and McDermott, A. E. (2001) The time scale of the catalytic loop motion in triosephosphate isomerase, *J. Mol. Biol. 310*, 259−270.
11. Joseph, D., Petsko, G. A., and Karplus, M. (1990) Anatomy of a conformational change: Hinged "lid" motion of the triosephosphate isomerase loop, *Science 249*, 1425−1428.
12. Derreumaux, P., and Schlick, T. (1998) The loop opening/closing motion of the enzyme triosephosphate isomerase, *Biophys. J. 74*, 72−81.
13. Massi, F., Wang, C., and Palmer, A. G., III (2006) Solution NMR and computer simulation studies of active site loop motion in triosephosphate isomerase, *Biochemistry 45*, 10787−10794.
14. Desamero, R., Rozovsky, S., Zhadin, N., McDermott, A., and Callender, R. (2003) Active site loop motion in triosephosphate isomerase: T-Jump relaxation spectroscopy of thermal activation, *Biochemistry 42*, 2941−2951.

15. Blacklow, S. C., Raines, R. T., Lim, W. A., Zamore, P. D., and Knowles, J. R. (1988) Triosephosphate isomerase catalysis is diffusion controlled, *Biochemistry 27*, 1158−1167.
16. Lolis, E., Alber, T., Davenport, R. C., Rose, D., Hartman, F. C., and Petsko, G. A. (1990) Structure of yeast triosephosphate isomerase at 1.9-Å resolution, *Biochemistry 29*, 6609−6618.
17. Lolis, E., and Petsko, G. A. (1990) Crystallographic analysis of the complex between triosephosphate isomerase and 2-phosphoglycolate at 2.5-Å resolution: Implications for catalysis, *Biochemistry 29*, 6619−6625.
18. Guallar, V., Jacobson, M., McDermott, A., and Friesner, R. A. (2004) Computational modeling of the catalytic reaction in triosephosphate isomerase, *J. Mol. Biol. 337*, 227−239.
19. Jogl, G., Rozovsky, S., McDermott, A. E., and Tong, L. (2003) Optimal alignment for enzymatic proton transfer: Structure of the Michaelis complex of triosephosphate isomerase at 1.2-Å resolution, *Proc. Natl. Acad. Sci. U.S.A. 100*, 50−55.
20. Wang, C., Rance, M., and Palmer, A. G. (2003) Mapping chemical exchange in proteins with MW > 50 kD, *J. Am. Chem. Soc. 125*, 8968−8969.
21. Furth, A. J., Milman, J. D., Priddle, J. D., and Offord, R. E. (1974) Studies on the subunit structure and amino acid sequence of triose phosphate isomerase from chicken breast muscle, *Biochem. J. 139*, 11−22.
22. Sun, J., and Sampson, N. S. (1999) Understanding protein lids: Kinetic analysis of active hinge mutants in triosephosphate isomerase, *Biochemistry 38*, 11474−11481.
23. Loria, J. P., Rance, M., and Palmer, A. G. (1999) A TROSY CPMG Sequence for Characterizing Chemical Exchange in Large Proteins, *J. Biomol. NMR 15*, 151−155.
24. Igumenova, T. I., and Palmer, A. G., III (2006) Off-resonance TROSY-selected $R_{1\rho}$ experiment with improved sensitivity for medium- and high-molecular-weight proteins, *J. Am. Chem. Soc. 128*, 8110−8111.
25. Palmer, A. G., III, and Massi, F. (2006) Characterization of the dynamics of biomacromolecules using rotating-frame spin relaxation NMR spectroscopy, *Chem. Rev. 106*, 1700−1719.
26. Delaglio, F., Grzesiak, S., Vuister, G., Zhu, G., Pfeifer, J., and Bax, A. (1995) NMRPipe: A multidimensional spectral processing system based on UNIX pipes, *J. Biomol. NMR 6*, 277−293.
27. Goddard, T., and Kneller, D. G. (2005) *SPARKY 3*, University of California, San Francisco.
28. Cole, R., and Loria, J. P. (2002) Evidence for flexibility in the function of ribonuclease A, *Biochemistry 41*, 6072−6081.
29. Press, W. H., Flannery, B. P., Teukolsky, S. A., and Vetterling, W. T. (1986) *Numerical Recipes. The Art of Scientific Computing*, 2nd ed., Cambridge University Press, Cambridge, U.K.
30. Palmer, A. G., Kroenke, C. D., and Loria, J. P. (2001) Nuclear magnetic resonance methods for quantifying microsecond-to-millisecond motions in biological macromolecules, *Methods Enzymol. 339* (Part B), 204−238.
31. Kempf, J. G., and Loria, J. P. (2004) in *Protein NMR Techniques* (Downing, A. K., Ed.) pp 185−231, Humana Press, Totowa, NJ.
32. Ugurbil, K., Garwood, M., and Rath, A. R. (1988) Optimization of modulation functions to improve insensitivity of adiabatic pulses to variations in B_1 magnitude, *J. Magon. Reson. 80*, 448−469.
33. Garwood, M., and Ke, Y. (1991) Symmetric pulses to induce arbitrary flip angles with compensation of RF inhomogeneity and resonance offsets, *J. Magn. Reson. 94*, 511−525.
34. Mulder, F. A. A., de Graaf, R. A., Kaptein, R., and Boelens, R. (1998) An Off-resonance Rotating Frame Relaxation Experiment for the Investigation of Macromolecular Dynamics Using Adiabatic Rotations, *J. Magn. Reson. 131*, 351−357.
35. Kempf, J. G., Jung, J., Sampson, N. S., and Loria, J. P. (2003) Off-resonance TROSY ($R1\rho$ − R1) for quantitation of fast exchange processes in large proteins, *J. Am. Chem. Soc. 125*, 12064−12065.
36. Pervushin, K., Riek, R., Wider, G., and Wuthrich, K. (1997) Attenuated T2 relaxation by mutual cancellation of dipole-dipole coupling and chemical shift anisotropy indicates an avenue to NMR structures of very large biological macromolecules in solution, *Proc. Natl. Acad. Sci. U.S.A. 94*, 12366−12371.
37. Xu, X. P., and Case, D. A. (2001) Automated prediction of ^{15}N, $^{13}C\alpha$, $^{13}C\beta$ and $^{13}C'$ chemical shifts in proteins using a density functional database, *J. Biomol. NMR 21*, 321−333.
38. Davis, D. G., Perlman, M. E., and London, R. E. (1994) Direct measurements of the dissociation-rate constant for inhibitor-enzyme complexes via the $T_{1\rho}$ and T_2 (CPMG) methods, *J. Magn. Reson., Ser. B 104*, 266−275.
39. James, T. L., Matson, G. B., Kuntz, I. D., and Fisher, R. W. (1977) Rotating frame spin-lattice relaxation in the presence of an off-resonance radio frequency field. Investigation of intermediate molecular motions, *J. Magn. Reson. 28*, 417−426.
40. Jones, G. P. (1966) Spin-lattice relaxation in the rotating frame: Weak-collision case, *Phys. Rev. 148*, 332−335.
41. Akke, M., and Palmer, A. G. (1996) Monitoring Macromolecular Motions on Microsecond−Millisecond Time Scales by $R_{1\rho}-R_1$ Constant-Relaxation-Time NMR Spectroscopy, *J. Am. Chem. Soc. 118*, 911−912.
42. Akaike, H. (1973) in *Proceedings of the 2nd international symposium on information theory* (Petrov, B. N., and Csaki, F., Eds.) pp 267−281, Akademia Kiado, Budapest.
43. Devore, J. (2000) *Probability and Statistics for Engineering and the Sciences*, Brooks/Cole Publishing Co., Monterey, CA.
44. Banner, D. W., Bloomer, A. C., Petsko, G. A., Phillips, D. C., Pogson, C. I., and Wilson, I. A. (1975) Structure of chicken triosephosphate isomerase determined crystallographically at 2.5 Å resolution, *Nature 255*, 609−614.
45. Zhang, Z., Sugio, S., Komives, E. A., Liu, K. D., Knowles, J. R., Petsko, G. A., and Ringe, D. (1994) Crystal structure of recombinant chicken triosephosphate isomerase-phosphoglycohydroxamate complex at 1.8 Å resolution, *Biochemistry 33*, 2830−2837.
46. Kursula, I., and Wierenga, R. K. (2003) Crystal structure of triosephosphate isomerase complexed with 2-phosphoglycolate at 0.83-Å resolution, *J. Biol. Chem. 278*, 9544−9551.
47. DeLano, W. L. (2005) *MacPyMOL*, DeLano Scientific LLC, South San Francisco, CA.
48. Chenna, R., Sugawara, H., Koike, T., Lopez, R., Gibson, T. J., Higgins, D. G., and Thompson, J. D. (2003) Multiple sequence alignment with the Clustal series of programs, *Nucleic Acids Res. 31*, 3497−3500.
49. Rance, M., Loria, J. P., and Palmer, A. G. (1999) Sensitivity improvement of transverse relaxation-optimized spectroscopy, *J. Magn. Reson. 136*, 92−101.
50. Grzesiek, S., Stahl, S. J., Wingfield, P. T., and Bax, A. (1996) The CD4 determinant for downregulation by HIV-1 Nef directly binds to Nef. Mapping of the Nef binding surface by NMR, *Biochemistry 35*, 10256−10261.

BI700344V